

PCCP

Accepted Manuscript



This is an *Accepted Manuscript*, which has been through the Royal Society of Chemistry peer review process and has been accepted for publication.

Accepted Manuscripts are published online shortly after acceptance, before technical editing, formatting and proof reading. Using this free service, authors can make their results available to the community, in citable form, before we publish the edited article. We will replace this *Accepted Manuscript* with the edited and formatted *Advance Article* as soon as it is available.

You can find more information about *Accepted Manuscripts* in the [Information for Authors](#).

Please note that technical editing may introduce minor changes to the text and/or graphics, which may alter content. The journal's standard [Terms & Conditions](#) and the [Ethical guidelines](#) still apply. In no event shall the Royal Society of Chemistry be held responsible for any errors or omissions in this *Accepted Manuscript* or any consequences arising from the use of any information it contains.

Excited state deactivation pathways of neutral/protonated anisole and p-fluoroanisole: A

Theoretical study

Reza Omidyan* and Hajar Rezaei

Department of Chemistry, University of Isfahan, 81746-73441 Isfahan, Iran

Abstract

The potential energy profiles of neutral and protonated anisole and p-fluoroanisole, at different electronic states have been investigated extensively by RI-MP2 and RI-CC2 methods. The calculations reveal that relaxation dynamics in protonated anisole and p-fluoroanisole is essentially different from that of neutral analogues. In neutral anisole/p-fluoroanisole, the $^1\pi\sigma^*$ state, plays the vital relaxation role along the O-CH₃ coordinate, yielding the CH₃ radical. For both of these molecules, the calculations indicate a conical intersections (CIs) between ground and excited state potential energy (PE) curves, hindered by a small barrier, and providing non-adiabatic gates for radiation-less deactivation to ground state. Nevertheless, for protonated cases, besides the prefulvenic deformation of benzene ring, it has been predicted that the lowest $^1(\sigma,n)\pi^*$ state along the bond angle of C-O-C plays an important role in photochemistry and relaxation dynamics. The S₁, S₀ PE profiles of protonated anisole along with the former reaction coordinate (out-of-plane deformation), show a barrierless relaxation pathway, which can be responsible for ultrafast deactivation of excited system to the ground state via the low-lying S₁/S₀ conical intersection. Moreover, the later reaction coordinate in protonated species; (C-O-C angle from 120°-180°) is consequently accompanied with the bond cleavage of C-OCH₃ at the $^1(\sigma,n)\pi^*$ state, hindered by a barrier of ~0.51 eV, can be responsible for relaxation of excited systems by significant excess energy ($h\nu \geq 5$ eV).

Furthermore, according to the RI-CC2 calculated results, different effects on the S₁-S₀ electronic transition energy of anisole and p-fluoroanisole upon to protonation have been predicted. The first electronic transition of anisole and p-fluoroanisole shift by ~0.3 and 1.3 eV to the red respectively due to protonation.

* Corresponding author, E-mail: r.omidyan@sci.ui.ac.ir, reza.omidyan@u-psud.fr, Fax: (+98) 311 6689732

Keywords: Anisole, Excited States, MP2 and CC2 methods, Relaxation Channels, Conical Intersections.

1-Introduction

Protonated aromatic molecules (denoted AH^+) appear frequently as reactive intermediates in chemical and biochemical reactions^{1, 2}. The characterization of AH^+ has a vital role to understand and possibly control the dynamics and selectivity of chemical processes¹⁻³. Since of recent advances on laser spectroscopy and computational methods, especial attentions have been paid to protonated aromatic molecules⁴⁻¹¹. As a commonly concluding remark of recent studies on the AH^+ in gas phase, it has been highlighted that a red shift effect on the S_1-S_0 electronic transition is the main consequence of protonation of such molecules^{4-6, 12-14}. Recently an experimental study has been reported by the research group of C. Jouvet on protonated Indole¹², where a red shift effect on electronic transition of protonated Indole; (as a heteroaromatic hydrocarbon) has been confirmed. In contrary, our recent investigation on protonated 2-Pyridone showed that a blue shift effect on the S_1-S_0 electronic transition as a consequence of protonation of heteroaromatic compounds is also possible¹⁵.

Moreover, photochemistry of organic compounds plays an essential role in our day-to-day lives. Our molecular building blocks readily absorb ultraviolet radiation. However these molecules display a large degree of photostability¹⁶, arising from quenching of photochemical reactions through ultrafast non-radiative processes imparting a high degree of photostability to these building blocks of life¹⁷⁻¹⁹. The dynamics of photoinduced bond cleavages in heteroatom containing aromatic molecules like azoles, phenols and so forth^{16, 20-24}, have been the focus of intensive recent studies, both from their perspective of fundamental photochemistry and because many of such species, constitute the chromophores in larger biochemically relevant species (e.g. in the DNA nucleobases)^{18, 22-26}. According to recent investigations, it has been established that dissociative $^1\pi\sigma^*$ is a key players in the photo resistive properties of chromophores of aromatic amino acids and DNA bases¹⁹⁻²². Spectroscopic detection of H-atom appearance times and velocity distributions are indirect evidence for relaxation along the $^1\pi\sigma^*$ state²³. According to recent reports of M. N. Ashfold and coworkers, the H atom photofragment translational spectroscopy (HRA-PTS) studies of the UV photodissociation of phenol, confirms O–H bond cleavage following excitation at energies both below and above the conical intersection between

the S_1 and S_2 potential energy surfaces²⁴⁻²⁹. Although several experimental and theoretical reports have been directed towards $^1\pi\sigma^*$ states in hydrides (X-H)^{24, 26-29}, much less effort has been directed at studying these dissociative states localized on other coordinates such as X-C. The velocity map ion imaging (VMI) work of A. G. Sage et al.³⁰ was the first to identify the role of $^1\pi\sigma^*$ state induced bond dissociation in non-hydride heteroaromatic systems. Using time-resolved velocity map imaging (TR-VMI), it has been suggested that CH_3 elimination with high kinetic energy is justified only by a direct dissociation of X- CH_3 bond of excited system involving a $^1\pi\sigma^*$ state³⁰. Also, experimental and theoretical study of D. J. Hadden et al.³¹ on mequinol (methoxy-phenol), reveal a competing dynamics along the $^1\pi\sigma^*$ of O-H and $^1\pi\sigma^*$ of O- CH_3 surfaces and a strong excitation wavelength dependence upon the tendency for either O-H or O- CH_3 bond cleavage, respectively.

In contrast to the neutral aromatic hydrocarbons, which have been the subjective of numerous studies so far^{19, 25, 26, 30-40}, rarely reports have been devoted on photophysics and photochemistry of protonated aromatic compounds^{15, 41, 42}. According to the report of Rode et al.⁴¹ on photophysics of protonated benzene, it has been suggested that the ring deformations on the region where the excess proton locates, leads the excited system to the ground by a conical intersection between the S_1/S_0 PESs. This conical intersection can be responsible for ultrafast deactivation of excited system via internal conversion.

In present study, protonation effect on the electronic transition energies and photophysical behavior of anisole and p-fluoroanisole will be addressed based on the CC2/MP2 methods. Anisole has been the subjective of several experimental⁴³⁻⁶⁰ and theoretical⁶¹⁻⁶³ studies. The high resolution S_1 - S_0 electronic excitation spectrum of anisole has been recorded in a molecular beam experiment by F. Lahmani et al.⁶⁴ and later by C. G. Eisenhardt et al.⁴⁸. It has been shown that the band origin of S_1 - S_0 electronic transition of anisole lies on the 36386 cm^{-1} (4.512 eV). Using the high accuracy rotational spectrum of anisole, the planarity of molecule in both of the ground and excited state has been clearly demonstrated^{46, 52}. In addition, the rotationally resolved S_1 - S_0 electronic spectra of anisole and its hydrogen bonded complex containing one water molecule have been obtained by J. W. Ribblett et al.⁵⁹. Also D. Xiao and coworkers⁶⁵ recorded the vibronic structure of p-fluoroanisole in the first excited state (S_1) with mass selected resonance-enhanced two photon ionization spectroscopy. The band origin of S_1 - S_0 transition of p-fluoroanisole has been measured to 35149 cm^{-1} (4.358 eV), which is red-shifted

by 1234 cm^{-1} with respect to that of anisole. Also, an extensive experimental study on the photophysics of neutral anisole has been performed by D. J. Hadden et al.⁵³. Using the TR-VMI experiment, they demonstrated that the CH_3 elimination, with high kinetic energy, is the only fragment eliminates due to direct dissociation involving a $^1\pi\sigma^*$ state⁵³.

Our paper is organized as follows: after summarizing the computational methods, we present ground- and excited-state optimized structures, protonated isomers and vertical/adiabatic transition energies. Then, we discuss and explain the deactivation pathways of excited species of neutral/protonated anisole and p-fluoroanisole. We start with the neutral structures because they form a basis for understanding of protonated species. The CC2 is method of choice because it gives reasonable results for medium size organic molecules, either in bare form or in their complex structures (e. g with water and ammonia) for a moderate computational time^{5, 14, 15, 42, 66-69}.

2- Computational details:

The “*ab initio*” calculations have been performed with the TURBOMOLE program suit^{70, 71}, making use of the resolution-of-identity⁷² (RI) approximation for the evaluation of the electron repulsion integrals. The equilibrium geometry of all systems at the ground state has been determined at the MP2 (Moller-Plesset second order perturbation theory) level^{73, 74}. Excitation energies and equilibrium geometry of the lowest excited singlet states have been determined at the RI-CC2 (the second-order approximate coupled-cluster method)⁷⁵⁻⁷⁹. The Dunning’s correlation consistent split-valence double- ζ basis set (cc-pVDZ)^{80, 81} and the augmented cc-pVDZ by diffuse functions on all atoms (aug-cc-pVDZ)⁸² have been employed.

All of the neutral and protonated systems are of C_s symmetry in the ground state. With exception of few calculations relevant to the PE profiles; (will be addressed evidently), the C_s symmetry of systems was maintained for geometry optimization of ground and excited states as well. Within the C_s point group the wave function of the ground state and S_1 ($^1\pi\pi^*$) state transform according to the A' representation and thus they are more distinguishable either with the $^1\pi\sigma^*$ in neutral molecules, or with the $^1(\sigma,n)\pi^*$ excited state in protonated homologues; (both belong to the A'' symmetry representation). The numbering pattern of the carbon atoms is shown in Figure 1.

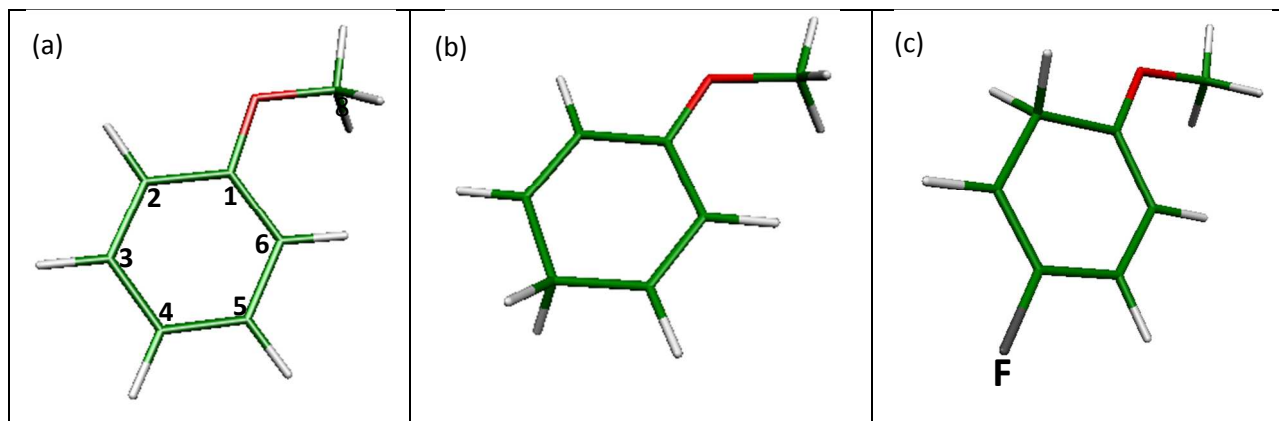


Figure 1: Optimized geometries of: (a) Neutral anisole and numbering pattern (b) the most stable isomer of protonated anisole (C4 isomer) (c) the most stable isomer of protonated p-fluoroanisole (C2 isomer).

3- Results and Discussions:

3-A: Geometry and electronic structures:

3-A- I: Protonated isomers of anisole and p-fluoroanisole:

The ground-state equilibrium structure of anisole and p-fluoroanisole have been determined by several authors and need not to be discussed here^{45, 46, 61, 63, 83}. We only present the results of calculations relevant to protonated species. Similar to protonated phenol⁸⁴, there are several protonation sites on neutral anisole and p-fluoroanisole corresponding to different positions of carbon atoms on benzene rings. However, to precisely find the relative energy of protonated isomers, the MP2 geometry optimization for all protonated isomers of anisole and p-fluoroanisole have been done. There are five protonated isomers for anisole and four different isomers for protonation of p-fluoroanisole, corresponding to different carbon sites on two molecules (See ESI file for the xyz coordinates). The relative energy of isomers associated with protonation of anisole and p-fluoroanisole have been presented respectively in Table 1 and Table 2. Also, Figure 1 shows the optimized geometries and numbering scheme of neutral anisole/p-fluoroanisole.

Protonated Isomer [Ground state relative energy /eV]	Vertical transitions /(eV)				Adiabatic transitions /(eV)			
	cc-pVDZ		aug-cc-pVDZ		cc-pVDZ		aug-cc-pVDZ	
	S ₁	S ₂	S ₁	S ₂	S ₁	S ₂	S ₁	S ₂
C2[0.12]	3.71	5.48	3.62 (0.221)	5.42 (0.002)	3.41	*	3.30	*
C3[0.77]	2.98	4.74	2.96 (0.093)	4.70 (0.474)	2.65	4.37	2.60	3.89
C4[0.00]	4.77	5.25	4.70 (0.142)	5.17 (0.374)	4.38	*	4.30	*
C5[0.71]	2.95	4.75	2.95 (0.730)	4.71 (0.086)	2.60	4.95	2.55	3.91
C6[0.14]	3.79	5.61	3.71 (0.203)	5.56 (0.086)	3.50	*	3.40	*
Neutral anisole	5.00	6.22	4.48 (0.290)	5.37 (0.002)	4.80	5.95	4.64 # 4.512	4.99

Table 1: Excited transition energies (vertical and adiabatic), of neutral and protonated anisole, computed at the MP2/CC2 levels with two different basis sets. The values in parenthesis correspond to the oscillator strength. #The experimental values for the 0-0 band of S₁-S₀ transition of neutral anisole, has been taken from Ref. ⁶⁴. *The S₂ geometry optimization for some of protonated isomers (denoted by * sign), doesn't converge either for strong degeneracy of a' 2 and a' 1 (in C4) or for the strong geometry deformations upon to the a''1 state (in the C2 and C6 isomers).

According to the MP2/CC2 results, the C4 isomer has been found to be the most stable isomer produced from protonation of anisole (or the lowest in energy compare with the other isomers) and the isomer for which the excess proton located on C3, has the highest ground state energy (+0.77 eV higher than the C4 isomer, at the RI-CC2/aug-cc-pVDZ level of theory, see Fig. 1 for the numbering pattern and the ESI file for more information). In addition, no stable C1 structure from protonation of anisole has been found, and all efforts to optimize structures of the C1 type isomer converge via barrierless proton transfer to the more stable C2 structure. Hence, we do not consider the C1 isomer in detail further. As shown in Table 1, the ground state energetic level of other isomers is 0.12-0.77 eV more than that of C4 isomer.

Protonated Isomer [Ground state relative energy /eV]	Vertical transitions /(eV)				Adiabatic transitions /(eV)			
	cc-pVDZ		aug-cc-pVDZ		cc-pVDZ		aug-cc-pVDZ	
	S ₁	S ₂	S ₁	S ₂	S ₁	S ₂	S ₁	S ₂
C2 [0.00]	3.40	5.43	3.33 (0.187)	5.38 (0.002)	3.13	*	3.03	*
C3 [0.47]	2.76	4.82	2.71 (0.092)	4.77 (0.055)	2.42	4.32	2.34	4.24
C5 [0.35]	2.81	4.81	2.77 (0.071)	4.77 (0.138)	2.46	4.35	2.37	4.25
C6 [0.02]	3.50	5.57*	3.43 (0.162)	5.53 (0.0009)	3.20	*	3.11	*
Neutral-F-Anisole	4.81	6.29	4.66 (0.048)	5.33 (0.0006)	4.60	6.04	4.42 #4.358	5.10

Table 2: Excited transition energies (vertical and adiabatic), of neutral and protonated *p*-fluoroanisole, computed at the MP2/CC2 levels with two different basis sets. The values in parenthesis correspond to the oscillator strength. [#]The experimental values for the 0-0 band of *S*₁-*S*₀ transition of *p*-fluoroanisole, has been taken from Ref.⁶⁵. *The *S*₂ geometry optimization for C2 and C5 protonated isomers doesn't converge since of the strong geometry deformations at *S*₂ (*a''1*) state.

Furthermore, according to the MP2/CC2 calculations on protonated *p*-fluoroanisole, it has been predicted that C2 isomer is the most stable isomer produced from protonation of *p*-fluoroanisole, and the isomer producing by locating of proton on C3, has the highest ground state energy (+0.47 eV higher than the C2 isomer, at the RI-CC2/aug-cc-pVDZ level of theory). As shown in Table 2, the ground state energetic level of other isomers is 0.02-0.47 eV more than that of C2. Although, protonation of *p*-fluoroanisole at the carbon site of C1, leads to a local minimum, it is considerably less stable by $\Delta E \approx 95 \text{ kJ mol}^{-1}$ (compared to the most stable C2 isomer). Since, the small barriers enable isomerizations of C1 toward C2 or C6, we didn't consider C1, for more calculations (for more applicable information, see Ref.⁸⁵ and references therein).

The MP2/aug-cc-pVDZ calculation, obtained 8.77 eV (855.8 kJ mol⁻¹) for proton affinity of anisole which is in well agreement with corresponding experimental value of 8.70 eV (839.6 kJ mol⁻¹) reported by E. Hunter and S. Lias⁸⁶. Also at the same level of calculation, proton affinity of p-fluoroanisole has been calculated to 8.41 eV (811.0 kJ mol⁻¹) which is comparable to the experimental value of 795 kJ mol⁻¹ (8.23 eV) reported by B. Bogdanov et al⁸³.

3-A-II: Vertical and adiabatic transition energies of neutral and protonated anisole/p-fluoroanisole

In order to compare the excitation transition energies of protonated anisole and p-fluoroanisole with those of neutral analogues, we calculated adiabatic and vertical excitation energies for the lowest singlet electronic transitions. The calculated results of the two lowest lying transitions (S_1 , S_2) are presented in Table 1 and Table 2. Vertical transition energies have been calculated on the optimized geometry of ground state while the adiabatic transition energies have been determined based on the relevant excited state geometry optimized. Further details on the vertical excitation energies, oscillator strengths and configuration of involving molecular orbitals are presented in Table SM2 of ESI file. According to the results of CC2/aug-cc-pVDZ calculations for protonated anisole and p-fluoroanisole, the first $^1A'$ excited state corresponds to the S_1 - S_0 electronic transition, while the first $^1A''$ state corresponds either to the second (S_2 - S_0 , in C2 and C6 isomers) or to the third electronic transition (S_3 - S_0 , in C3, C4, C5 isomers). In both of neutral anisole and p-fluoroanisole, the $^1A''$ state corresponds to the second electronic transition (S_2 - S_0). In contrast to the $^1A'$ excited state, upon which, no important geometry deformation at the CC2 level of optimization has been predicted, geometry optimization at $^1A''$ excited state, undergoes to considerable deformation on the structure of neutral and protonated species. In Table 3, the optimized geometry of the most stable protonated isomers of anisole and p-fluoroanisole at ground and excited states as well as their neutral analogues have been presented. As shown, the CC2 geometry optimization of $^1A''$ excited state, in neutral anisole is accompanied with significant lengthening of O-CH₃; (bond cleavage of O-CH₃). Also, optimization the geometry of protonated species at $^1A''$ excited state, brings apart the bond-angle opening of COCH₃; (and consequently the bond cleavage of C-OCH₃). Since of such large deformations in the geometry of at $^1A''$ excited state, the CC2 method doesn't converge and we couldn't report the corresponding adiabatic transition energy values in Table 1 and Table 2.

The frontier molecular orbitals (MOs) of neutral and protonated anisole and p-fluoroanisole (most stable isomers) are shown in Table 4. From the RI-CC2 calculations, the S_1 ($^1A'$) state of protonated anisole (C4 isomer) corresponds to the orbital transition from HOMO to LUMO; (HOMO and LUMO respectively indicate to the highest occupied molecular orbital and the lowest unoccupied molecular orbital).

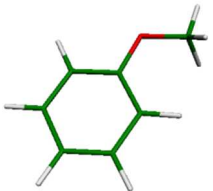
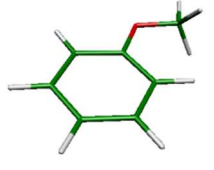
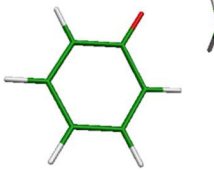
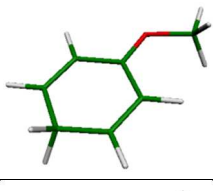
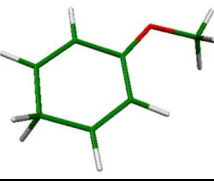
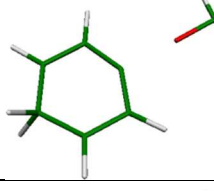
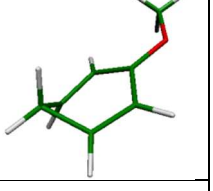
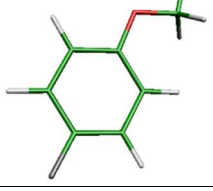
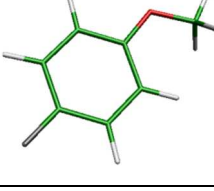
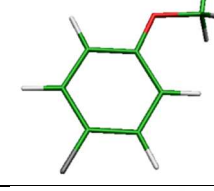
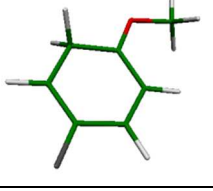
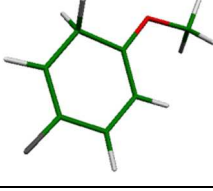
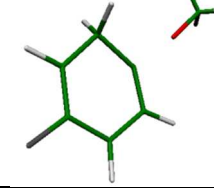
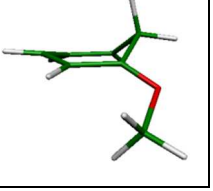
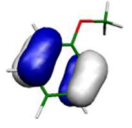
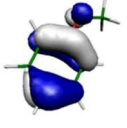
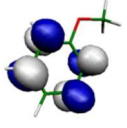
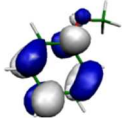
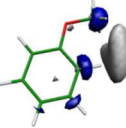
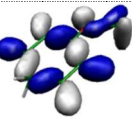
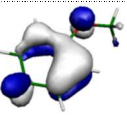
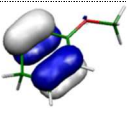
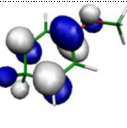
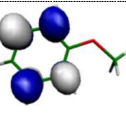
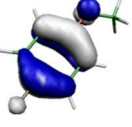
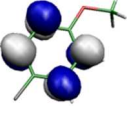
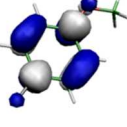
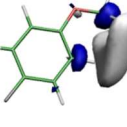
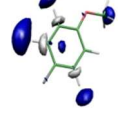
	S_0	S_1 ($^1A'$)	$^1A''$ (S_2 or S_3)	S_1 (without C_s symmetry)
Anisole				---
Protonated anisole (C4 isomer)				
p-fluoroanisole				---
Protonated p-fluoroanisole (C2 isomer)				

Table 3: Optimized geometry structures of neutral/protonated anisole and p-fluoroanisole. In the last column, the optimized geometry of protonated species, at the S_1 excited state, without the C_s symmetry constraint, has been shown.

As shown in Table 4, the Homo orbital of C4 protonated isomer is a π orbital and its Lumo is a π^* , thus, the S_1 state of C4 protonated isomer of anisole has the $^1\pi\pi^*$ nature. Also, the S_2-S_0 electronic transition; (the second A' state), arising from (Homo-1)-Lumo electronic transition, has the $^1\pi\pi^*$ character, while, the S_3-S_0 (the first A'' state) corresponds to the (Homo-2)-Lumo transition. As shown in Table 4, the Homo-2 orbital contains a combination of n_o (non-bonding orbital on oxygen atom) and σ (located on the benzene ring).

Thus the first A'' electronic transition of C4, protonated anisole has $^1(\sigma,n)\pi^*$ nature. As the same as protonated anisole, in protonated p-fluoroanisole, the S_1 and S_2 ($1A'$ and $2A'$) have $^1\pi\pi^*$ nature while the S_3 ($1A''$) has $^1(\sigma,n)\pi^*$ character. As it will be discussed in the next sections, the $1A''$ $^1(\sigma,n)\pi^*$ excited state has a vital role in the photochemistry of protonated anisole and p-fluoroanisole.

However, in neutral anisole and p-fluoroanisole, the S_1-S_0 ($1A'$) corresponds mostly to single electronic transition from Homo to Lumo which has the $^1\pi\pi^*$ nature and the S_2-S_0 ($1A''$), corresponds to Homo-Lumo+2 electronic transition which has the $^1\pi\sigma^*$ character (see Table 4).

	H-1	H	L	L+1	L+2
Anisole					
Protonated anisole (C4 isomer)					
p-fluoroanisole					
Protonated	H-2	H-1	H	L	L+1

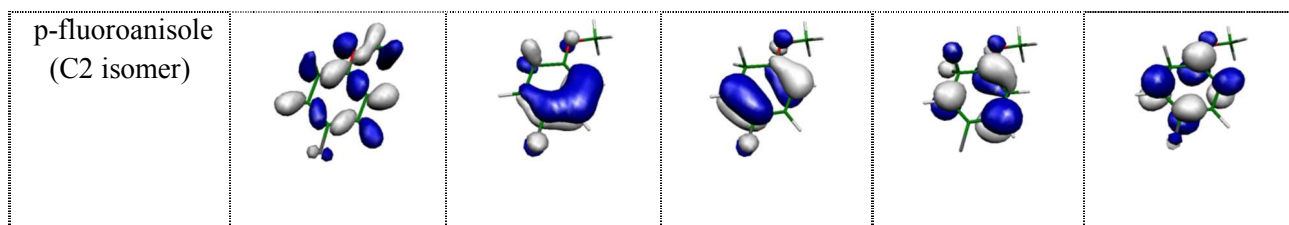


Table 4: Frontier MOs of neutral and protonated anisole/p-fluoroanisole. Only the MOs which have the prominent contribution on the S_1 and S_2 (or S_3) electronic transitions have been shown. Also, H and L respectively indicate to Homo and Lumo orbitals.

Comparison the adiabatic transition energies of S_1 - S_0 ($^1A'$) transition for protonated isomers and the one of neutral anisole (4.64 eV at the same level of theory and experimental value of 4.512 eV for 0-0 band of anisole reported by F. Lahmaini et al.⁶⁴), it can be concluded that protonation is accompanied with red shift effect on S_1 - S_0 transition energy of anisole by at least 0.3 eV. This effect in protonated p-fluoroanisole is more pronounced which is 1.25-2.00 eV. Inspection of calculated adiabatic transition energies for protonated anisole and also p-fluoroanisole (Table 1 and Table 2), it is seen that electronic transitions of S_1 - S_0 ($^1A'$) of protonated anisole with $^1\pi\pi^*$ character, lies in the UV-Vis range (4.30-3.03 eV respectively for C4 and C2 protonated isomers), while this transition in protonated p-fluoroanisole lies only in the visible (2.34-3.11 eV) as well.

3-B. Photophysical behavior: Potential energy profiles and internal conversions:

3-B-1. Neutral anisole:

The photophysics of anisole has been experimentally studied by several groups^{49, 53, 55, 60, 87, 88}. It has been clearly stated by Tseng⁸⁸ and later by Hadden⁵³ that the CH_3 elimination is the sole dissociation channel for the anisole at 193 and 248 nm. To our knowledge, there is no theoretical-exploration report on photophysics of anisole and fluoroanisole. Thus, we have investigated the relaxation channels in neutral anisole as well as p-fluoroanisole at the CC2/MP2 levels of theory. The potential energy profiles for both cases (neutral and protonated anisole) have been determined and the results have been presented in Figure 2 (a) and (b).

In Figure 2-a, the CC2 PE profiles calculated along the minimum-energy path (MEP) for detachment of methyl group (CH_3) from of neutral anisole are presented. The PE profiles have been calculated for an elongation of the $d(\text{O}-\text{CH}_3)$ stretching coordinate. For a given value of stretching coordinate $d(\text{O}-\text{CH}_3)$, all remaining coordinates have been optimized either for the $^1\pi\pi^*$ or $^1\pi\sigma^*$ excited states, under C_s symmetry. For clarity, only the lowest $^1\pi\pi^*$, and $^1\pi\sigma^*$ states and the electronic ground state are shown in Fig. 2. The excited states geometries have been optimized along this reaction path, while the ground-state energy is computed at the $^1\pi\sigma^*$ optimized geometries. From inspection of results presented in Figure 2-a, it is also seen that the PE profiles of the ground state and the lowest valence $^1\pi\pi^*$ excited state rise with increasing O- CH_3 distance, while the PE profile of the $^1\pi\sigma^*$ state is essentially repulsive. The repulsive $^1\pi\sigma^*$ PE profile crosses with $^1\pi\pi^*$ state at the middle of reaction path. In a multidimensional picture, the $^1\pi\pi^*$ - $^1\pi\sigma^*$ curve crossings in Figure 2-a, develops into the conical intersections (CIs). Because, the potential energy curves of the different electronic states ($^1\pi\pi^*$ and $^1\pi\sigma^*$), have been determined independently at different geometry optimizations, the energetic position of these CIs cannot be precisely determined from Fig. 2. Nevertheless, the CC2 calculations are reliable^{38, 89, 90}, and our results relevant to the CIs are good signs for the region of conical intersections qualitatively.

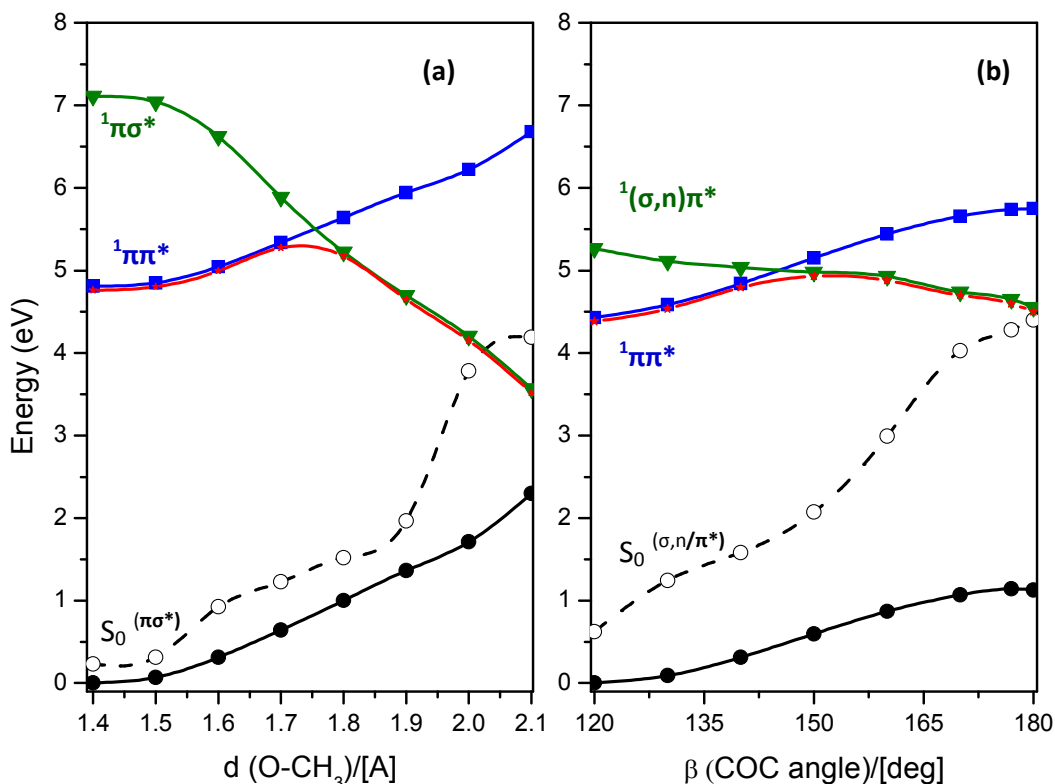


Figure 2: CC2 PE profiles of (a) neutral and (b) protonated anisole (*C4* isomer) in the electronic ground state (circles), the lowest $^1A'$ excited state (squares), the lowest $^1A''$ state (triangles), as a function of O-CH₃ coordinate in the neutral and COC angle in protonated case. The red-color curves in both panels represent the PE profile of S_1 state without C_s symmetry constraint.

The resulting lower adiabatic PE sheet of the coupled $^1\pi\pi^*$ - $^1\pi\sigma^*$ states exhibits a small barrier in the vicinity of the conical intersection. We have evaluated this barrier by breaking the C_s symmetry of the system; (to allow vibronic coupling between $^1\pi\pi^*$ and $^1\pi\sigma^*$ states). The barrier has been determined amount to 0.51 eV, consequently, a wave packet prepared in the $^1\pi\pi^*$ state by optical excitation with sufficient excess energy (≈ 0.51 eV) will bypass this barrier and then evolve on the $^1\pi\sigma^*$ surface. The low-energy part of the $^1\pi\pi^*$ surface is separated from the region of strong non-adiabatic interactions with the ground state by this barrier on the PE surface of the lowest excited singlet state. Moreover, the repulsive $^1\pi\sigma^*$ PE profile intersects the PE function of the ground state at an O-CH₃ distance of about 2.0 Å, resulting in another conical intersection

(CI). This CI is expected to lead the excited system to an ultrafast internal conversion to the ground state.

These results are in well agreement with the experimental reports of Hadden⁵³ and Tseng⁸⁸, where the $-\text{CH}_3$ fragment has been observed at laser wavelength of 193 and 248 nm with sufficient kinetic energy. When the photon energy with this range of wavelength (193-248 nm; 6.43-5 eV) is exposed to anisole, the excited system has sufficient energy to bypass the barrier of $^1\pi\pi^* \rightarrow ^1\pi\sigma^*$ evolution. After this barrier, the excited system may dissociate along the O- CH_3 bond: $\text{C}_6\text{H}_5\text{OCH}_3 \rightarrow \text{C}_6\text{H}_5\text{O} + \text{CH}_3$ producing the phenoxy and methyl radicals with the excess kinetic energy, or it decays to the ground state.

3-B-2. Protonated anisole (C4 isomer) under the C_s symmetry constraint:

In the C_s symmetry point group, the first and second electronic transitions (S_1 and S_2) of protonated anisole (C4 isomer), having the $^1\pi\pi^*$ nature, having A' representation while the third one (S_3 state) belongs the A'' representation and has electronic $^1(\sigma,n)\pi^*$ nature. Due to the different nature of the first A'' state in protonated anisole than that of neutral homologue, a different photochemical behavior for protonated anisole can be expected. Moreover, the optimized geometry of C4 protonated isomer of anisole at $S_3(A''-^1\sigma,n\pi^*)$ state shows drastic alterations in the C-O- CH_3 bond angle; (from 120° to 180°) and also in the C-O CH_3 bond length; (from 1.220 Å to 1.950 Å). Thus, a bond cleavage between the benzene ring and methoxy group can be the main consequence of UV excitation of protonated anisole (C4 isomer).

In order to determine the PE profiles of protonated anisole, either the COC bond angle (β) or the C-O CH_3 bond distance (d) can be considered as the reaction coordinate. Thus we have determined the PECs along with both reactions coordinates. The results along with the COC bond angle (β) has been presented in Figure 2-b, and the corresponding results along the C-O CH_3 bond length has been presented in the ESI file. As the same as neutral anisole, in determination of PE profiles (Fig. 2-b), only the lowest $1A'(^1\pi\pi^*)$, and $1A''(^1\sigma,n\pi^*)$ states and the electronic ground state have been presented. Along with the bond angle of C-O- CH_3 , as reaction coordinate, geometries of the excited states have been optimized, while the ground-state energy is computed at the $^1(\sigma,n)\pi^*$ optimized geometries. From of the results presented in Figure 2-b, this is clear that the PE profiles of the ground state and the lowest valence $^1\pi\pi^*$ excited state rise

with increasing C-O-CH₃ bond angle (from 120°-180°). This is while the PE profile of the ¹(σ,n)π* state is repulsive. However, the repulsive ¹(σ,n)π* PE profile crosses with ¹ππ* state at the middle of reaction path producing a conical intersection (CI) between ¹ππ*-¹σ,nπ* in a multidimensional picture. The resulting lower adiabatic PE sheet of the coupled ¹ππ*-¹σ,nπ* states will exhibit a barrier ≈0.56 eV in the vicinity of the conical intersection. Thus, a wave packet prepared in the ¹ππ* state by optical excitation with sufficient excess energy (≈5 eV) will bypass this barrier and then evolve on the ¹(σ,n)π* surface.

Also, it is seen in Figure 2-b that the repulsive ¹(σ,n)π* PE profile intersects the PE function of the ground state at an C-O-CH₃ angle of ~180°, resulting in another conical intersection. This conical intersection is expected to lead the excited system to an ultrafast internal conversion to the ground state. In addition, the CC2 PE profiles of ¹σ,nπ* along the C-OCH₃ bond distance (Fig. SM1, ESI file), shows a dissociative trend, which verifies the prediction of producing the OCH₃ radical photoproduct, upon to relaxation of the UV excited protonated anisole.

3-B-3: PE profiles of protonated anisole (C4 isomer without Cs symmetry constraint):

Extensive theoretical results on photochemistry of benzene has been reported by I. J palmer et al., where an out-of-plane distorted structure (e.i prefulvene) has been introduced as a photoproduct of benzene⁴⁰. The same result has been obtained for protonated benzene upon to the S₁ geometry optimization without symmetry restriction. Indeed, an out-of-plane deformation on the region where excess proton locates, occurs by the CC2 geometry optimization of protonated benzene^{41, 42}. It also has been well established that excited states of protonated benzene undergoes a very fast internal conversion and should be very short-lived^{41, 42}. Moreover, in the first excited state, the system has to lose its planar symmetry, and a conical intersection can be expectable with the ground state which arises along out-of-plane bending coordinates. As shown in Table 3 (last column on the right), such out-of-plane deformation happens in protonated anisole (C4, the most stable isomer) after the S₁ geometry optimization. This ring deformation can be a sign of curve crossing between S₁-S₀ in the PECs of protonated anisole as well as protonated benzene. Thus, we have investigated the PE curves of different electronic states of protonated anisole along with the ring deformation reaction coordinate. The potential energy profiles along the minimum energy paths (MEP) for torsion of the -CH₂; (the dihedral

angle of $C_4 - C_5 - C_6 - C_3$, see Fig. 1-a for numbering) in protonated anisole at the S_0/S_1 states have been calculated. The results are shown in Figure 3 (full curves). The coordinate-driven minimum-energy paths for out-of-plane deformation have been obtained by fixing the $\omega(C_4 - C_5 - C_6 - C_3)$ and optimizing the lowest S_1 state with respect to all other coordinates. The geometry optimizations have been performed with the CC2 method. The energies at the optimized geometries have been calculated at the CC2/cc-pVDZ level. In Fig. 3, the PE profiles of the S_0 state, calculated at the $^1\pi\pi^*$ optimized geometries (dashed lines with hollow squares), as well as at the S_0 optimized geometries, determined with the MP2 method (solid lines with filled squares), are also shown. Also, the $S_0^{(S1)}$ curve is rising by increasing the $\omega(C_4 - C_5 - C_6 - C_3)$, while, the energy profile of the S_1 state calculated along the S_1 reaction path ($S_1^{(S1)}$) indicates a barrier-free reaction coordinate which leads to the conical intersection. In the S_1 state, the MEP for the $-CH_2$ torsion could be determined with the exception of geometries which are very close to the S_1-S_0 conical intersection, where the CC2 iteration cycle fails to converge. Around 20° , the S_0/S_1 potential energy profiles cross with each other and obtain a conical intersection. This conical intersection mediates the radiation-less deactivation of the compounds after excitation of the lowest $^1\pi\pi^*$ state. Because, the relaxation of the $^1\pi\pi^*$ state of protonated anisole via $-CH_2$ twisting is barrier-free, this relaxation channel can be strongly in competition with that of C-OCH₃ bond cleavage. However, the former should be the main path for relaxation of excited system at the lower lying energy of excitation ($\Delta E \approx 4.5$ eV), though, the role of the later channel (C-OCH₃ bond cleavage) should be more pronounced when the system is excited by a photon having energy of more than 5.0 eV. After intersection point, the reaction coordinates (ω) increasing to more values the CI, leads the flat trend of $S_1^{(S1)}$ curve (data were not shown).

Figure 3-b shows the PE profiles of different electronic state of neutral anisole along with the ring twisting (dihedral angle of $\theta(C_4 - C_5 - C_6 - C_3)$). As seen, the rising trend of the S_1 state by increasing θ , shows that there is no barrier-free conical intersection in the PE curves of neutral anisole along with the ring distortion coordinate, verifying the difference between relaxation dynamics of neutral and protonated cases.

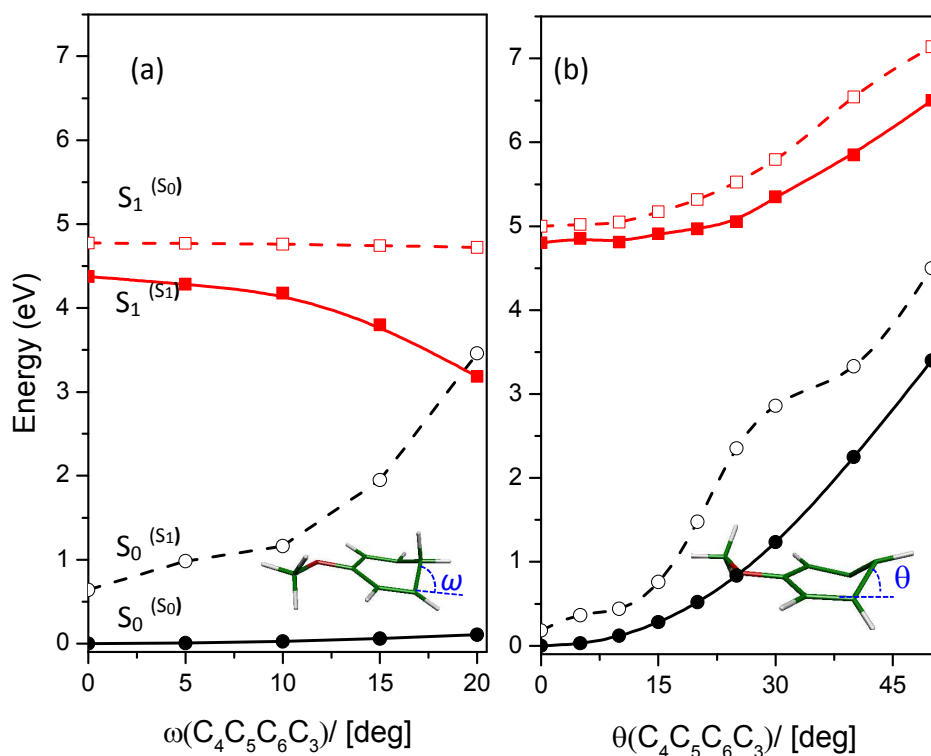


Figure 3: Potential energy curves of the S_0 state (circles) and the $S_1(\pi\pi^*)$ state (squares), of (a) protonated anisole and (b) neutral anisole, determined at the MP2,CC2/cc-pVDZ level for torsion of the $-\text{CH}_2$ and $-\text{CH}$ respectively in protonated and neutral anisole. The full lines represent the energy profiles of reaction paths determined in the same electronic state and the dashed lines show the energy profiles of reaction paths determined in the complementary electronic state.

3-B-4: Neutral and protonated p-fluoroanisole:

Similar to neutral anisole, the CC2 geometry optimization of p-fluoroanisole at the first $^1A''$ ($^1\pi\sigma^*$) state leads to the O-CH₃ bond cleavage. In Figure 4-a, the CC2 PE profiles calculated along the minimum-energy path for detachment of methyl group ($-\text{CH}_3$) from p-fluoroanisole are presented. From Figure 4-a, it is shown that the PE profiles of p-fluoroanisole behave in the same trend with those of protonated anisole. Also, the PE profile associated with the S_1 state, shows

roughly the same barrier (0.51 eV) as that of neutral anisole in Fig. 3 (a). Thus, photophysics of p-fluoroanisole shouldn't be essentially different from that of anisole.

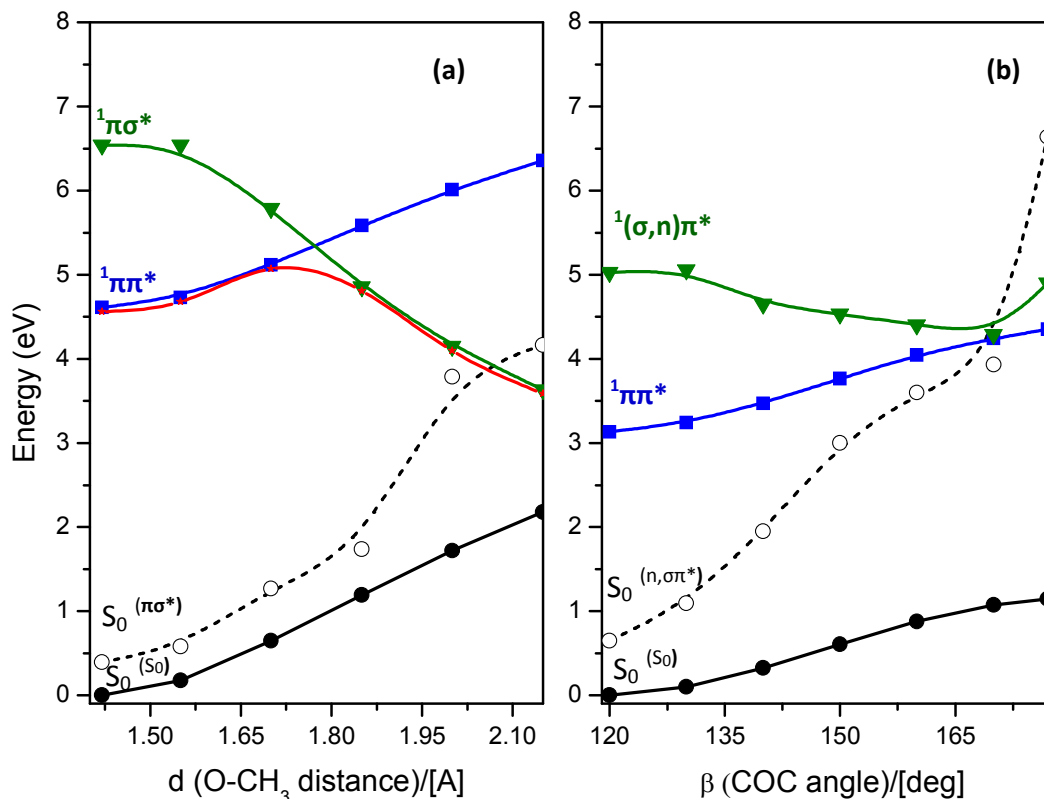


Figure 4: CC2 PE profiles of (a) neutral and (b) protonated p-fluoroanisole (C2 isomer) in the electronic ground state (circles), the lowest $^1A'$ excited state (squares), the lowest $^1A''$ state (triangles), as a function of the O-CH₃ coordinate in the neutral and COC angle in protonated cases. The red-color curve in panel (a), represents the PE profile of S_1 state without keeping the C_s symmetry constraint.

In Figure 4-b, the CC2 PE profiles calculated along the minimum-energy path for opening of C-O-CH₃ bond angle in protonated p-fluoroanisole has been presented. The PE profiles have been determined in the same approach, discussed in the previous section for protonated anisole. Although, the PE profiles of the ground state and the lowest valence $^1\pi\pi^*$ excited state rise with increasing C-O-CH₃ bond angle (from 120°-180°), and the PE profile of the $^1(\sigma,n)\pi^*$ state is repulsive, the decreasing trend of $^1(\sigma,n)\pi^*$ state by increasing the COC bond angle, is different

with that of corresponding state in protonated anisole. The smooth descent of $^1(\sigma,n)\pi^*$ along with the reaction coordinate causes removing the $\pi\pi^*-^1\sigma,n\pi^*$ conical intersection at the middle of reaction coordinate and move this CI to the end of reaction path (COC is 180°). Also, at the end of reaction path, (COC= 180°), the PE curve of $^1(\sigma,n)\pi^*$ crosses with that of ground state, producing a conical intersection which lead the excited system to relax toward ground state. According to the PE profiles of Fig. 4-b, one can conclude that the photoexcited protonated p-fluoroanisole with sufficient excess energy (≈ 5 eV), may either undergo photodissociation to produce OCH_3 radical or decay to the ground state via the conical intersection between $^1\sigma,n\pi^*-S_0$ and losing the absorbed energy to heat. Moreover, the dissociative nature of $^1(\sigma,n)\pi^*$ state along the C-OCH₃ distance verifies the suggestion of the C-OCH₃ bond breaking as a consequent photo-chemical reaction of protonated p-fluoroanisole as well (see Fig SM1 in ESI file).

4- Conclusion

The photochemistry of protonated anisole and p-fluoroanisole has been predicted to be essentially different from that of neutral analogues, since of differences in electronic states, reaction coordinates and photoproducts. It has been found that O-CH₃ coordinate is responsible for photochemistry of neutral anisole and p-fluoroanisole. The detachment of CH₃ in the S₁ state of neutral molecules, leads to a low-lying conical intersection of the S₁ and S₀ energy surfaces, providing the mechanism for efficient radiationless deactivation of the excited state back to the ground state or, alternatively, to dissociation of excited system (e.i to loss methyl group). These results are in agreement with previous experimental observations as well.^{53, 88}

On the other hand, for protonated anisole and p-fluoroanisole, similar to protonated benzene⁴¹, a prefulvenic deformation of benzene ring, has been found to lead the excited system from S₁ ($^1\pi\pi^*$) state toward the ground, via a barrierless conical intersection of $^1\pi\pi^*-S_0$ states. While, at the S₃ ($^1\sigma,n\pi^*$) state, the bond-angle opening of C-O-C, consequently accompanied with elongation of C-OCH₃ distance, can be responsible for photochemical process. The $^1(\sigma,n)\pi^*$ state in protonated anisole and p-fluoroanisole, predissociates the bound S₁($^1\pi\pi^*$) state, connecting the later to a conical intersection with the S₀ state, leading the excited systems either

back to the ground state or, bond cleavage of C-OCH₃, producing methoxy group as photoproduct.

According to theoretical differences between photochemistry of protonated and neutral anisole, it can be interesting if one investigates the relaxation dynamics of protonated anisole or p-fluoroanisole via the convenient experimental devices!.

Acknowledgment

The research council of *Isfahan University* is acknowledged for financial support. We are highly grateful to *Prof. C. Jouvet* from his valuable comments. Also, the use of computing facility cluster *GMPCS of the LUMAT* federation (FR LUMAT2764) for partially performance of our calculations is kindly appreciated.

References:

1. F. A. S. Carey, R. J., *Advanced Organic Chemistry*, Plenum Press: New York, 1995.
2. G. A. Olah, A. M. White and D. H. O'Brien, *Chem. Rev.*, 1970, **70**, 561-591.
3. H. H. Perkampus and E. Baumgarten, *Angew. Chem. Int. Edit.*, 1964, **3**, 776-783.
4. I. Alata, C. Dedonder, M. Broquier, E. Marceca and C. Jouvet, *J. Am. Chem. Soc.*, 2010, **132**, 17483-17489.
5. I. Alata, R. Omidyan, M. Broquier, C. Dedonder, O. Dopfer and C. Jouvet, *Phys. Chem. Chem. Phys.*, 2010, **12**, 14456-14458.
6. S. Chakraborty, R. Omidyan, I. Alata, I. B. Nielsen, C. Dedonder, M. Broquier and C. Jouvet, *J. Am. Chem. Soc.*, 2009, **131**, 11091-11097.
7. I. Garkusha, J. Fulara, A. Nagy and J. P. Maier, *J. Am. Chem. Soc.*, 2010, **132**, 14979-14985.
8. I. Garkusha, J. Fulara, P. J. Sarre and J. P. Maier, *J. Phys. Chem. A*, 2011, **115**, 10972-10978.
9. I. Garkusha, A. Nagy, J. Fulara, M. F. Rode, A. L. Sobolewski and J. P. Maier, *J. Phys. Chem. A*, 2013, **117**, 351-360.
10. U. J. Lorenz, N. Solcà, J. Lemaire, P. Maître and O. Dopfer, *Angew. Chem. Intern. Edit.*, 2007, **46**, 6714-6716.
11. A. Patzer, M. Zimmermann, I. Alata, C. Jouvet and O. Dopfer, *J. Phys. Chem. A*, 2010, **114**, 12600-12604.

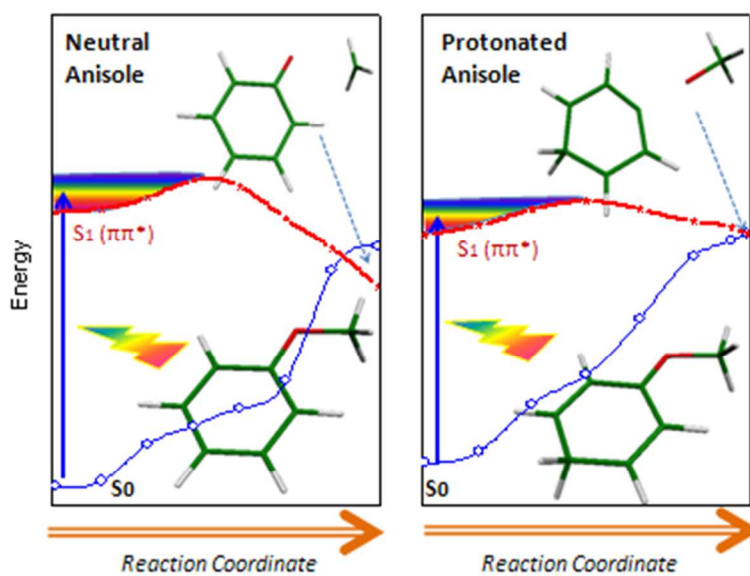
12. I. Alata, J. Bert, M. Broquier, C. Dedonder, G. Feraud, G. Gregoire, S. Soorkia, E. Marceca and C. Jouvét, *J. Phys. Chem. A*, 2013, **117**, 4420-4427.
13. I. Alata, M. Broquier, C. Dedonder, C. Jouvét and E. Marceca, *Chem. Phys.*, 2012, **393**, 25-31.
14. I. Alata, R. Omidyan, C. Dedonder-Lardeux, M. Broquier and C. Jouvét, *Phys. Chem. Chem. Phys.*, 2009, **11**, 11479-11486.
15. B. Saed and R. Omidyan, *J. Chem. Phys.*, 2014, **140**, 024315.
16. D. Creed, *Photochem. Photobiol.*, 1984, **39**, 537-562.
17. C. E. Crespo-Hernández, B. Cohen, P. M. Hare and B. Kohler, *Chem. Rev.*, 2004, **104**, 1977-2020.
18. T. J. Martínez, *Acc. Chem. Res.*, 2006, **39**, 119-126.
19. A. L. Sobolewski, W. Domcke, C. Dedonder-Lardeux and C. Jouvét, *Phys. Chem. Chem. Phys.*, 2002, **4**, 1093-1100.
20. A. L. Sobolewski and W. Domcke, *Chem. Phys.*, 2000, **259**, 181-191.
21. A. L. Sobolewski and W. Domcke, *J. Phys. Chem. A*, 2001, **105**, 9275-9283.
22. A. L. Sobolewski, W. Domcke, C. Dedonder-Lardeux and C. Jouvét, *Phys. Chem. Chem. Phys.*, 2002, **4**, 1093-1100.
23. G. A. Pino, A. N. Oldani, E. Marceca, M. Fujii, S.-I. Ishiuchi, M. Miyazaki, M. Broquier, C. Dedonder and C. Jouvét, *J. Chem. Phys.*, 2010, **133**, 124313.
24. G. A. King, T. A. Oliver, M. G. Nix and M. N. Ashfold, *J. Phys. Chem. A*, 2009, **113**, 7984-7993.
25. M. Ashfold, B. Cronin, A. Devine, R. Dixon and M. Nix, *Science*, 2006, **312**, 1637-1640.
26. M. N. Ashfold, G. A. King, D. Murdock, M. G. Nix, T. A. Oliver and A. G. Sage, *Phys. Chem. Chem. Phys.*, 2010, **12**, 1218-1238.
27. A. L. Devine, M. G. Nix, B. Cronin and M. N. Ashfold, *Phys. Chem. Chem. Phys.*, 2007, **9**, 3749-3762.
28. T. A. Oliver, G. A. King and M. N. Ashfold, *Phys. Chem. Chem. Phys.*, 2011, **13**, 14646-14663.
29. G. M. Roberts, D. J. Hadden, L. T. Bergendahl, A. M. Wenge, S. J. Harris, T. N. Karsili, M. N. Ashfold, M. J. Paterson and V. G. Stavros, *Chem. Sci.*, 2013, **4**, 993-1001.
30. A. G. Sage, M. G. D. Nix and M. N. R. Ashfold, *Chem. Phys.*, 2008, **347**, 300-308.
31. D. J. Hadden, G. M. Roberts, T. N. V. Karsili, M. N. R. Ashfold and V. G. Stavros, *Phys. Chem. Chem. Phys.*, 2012, **14**, 13415-13428.
32. M. N. Ashfold, A. L. Devine, R. N. Dixon, G. A. King, M. G. Nix and T. A. Oliver, *P. Natl. Acad. Sci. USA*, 2008, **105**, 12701-12706.

33. G. M. Roberts, D. J. Hadden, L. T. Bergendahl, A. M. Wenge, S. J. Harris, T. N. V. Karsili, M. N. R. Ashfold, M. J. Paterson and V. G. Stavros, *Chem. Sci.*, 2013, **4**, 993-1001.
34. A. Sobolewski, C. Woywod and W. Domcke, *J. Chem. Phys.*, 1993, **98**, 5627.
35. A. L. Sobolewski and L. Adamowicz, *J. Chem. Phys.*, 1995, **102**, 5708.
36. A. L. Sobolewski and L. Adamowicz, *J. Phys. Chem.*, 1996, **100**, 3933-3941.
37. A. L. Sobolewski and W. Domcke, *Chem. Phys. Lett.*, 1999, **315**, 293-298.
38. A. L. Sobolewski, W. Domcke and C. Hättig, *J. Phys. Chem. A*, 2006, **110**, 6301-6306.
39. A. L. Sobolewski, D. Shemesh and W. Domcke, *J. Phys. Chem. A*, 2008, **113**, 542-550.
40. I. J. Palmer, I. N. Ragazos, F. Bernardi, M. Olivucci and M. A. Robb, *J. Am. Chem. Soc.*, 1993, **115**, 673-682.
41. M. F. Rode, A. L. Sobolewski, C. Dedonder, C. Jouvet and O. Dopfer, *J. Phys. Chem. A*, 2009, **113**, 5865-5873.
42. B. Saed and R. Omidyan, *J. Phys. Chem. A*, 2013, **117**, 2499-2507.
43. M. Arivazhagan, N. K. Kandasamy and G. Thilagavathi, *Indian J. Pure App. Phys.*, 2012, **50**, 299-307.
44. F. Bayrakceken, S. Aktas, M. Toptan and A. Unlugedik, *Spectrochim. Acta A*, 2003, **59**, 135-138.
45. M. Dal Colle, G. Distefano, D. Jones and A. Modelli, *J. Phys. Chem. A*, 2000, **104**, 8227-8235.
46. O. Desyatnyk, L. Pszczolkowski, S. Thorwirth, T. M. Krygowski and Z. Kisiel, *Phys. Chem. Chem. Phys.*, 2005, **7**, 1708-1715.
47. C. G. Eisenhardt, A. S. Gemechu, H. Baumgartel, R. Chelli, G. Cardini and S. Califano, *Phys. Chem. Chem. Phys.*, 2001, **3**, 5358-5368.
48. C. G. Eisenhardt, G. Pietraperzia and M. Becucci, *Phys. Chem. Chem. Phys.*, 2001, **3**, 1407-1410.
49. S. Faust, T. Dreier and C. Schulz, *Appl. Phys. B-Lasers O.*, 2013, **112**, 203-213.
50. C. Gellini, L. Moroni and M. Muniz-Miranda, *J. Phys. Chem. A*, 2002, **106**, 10999-11007.
51. A. S. Gemechu, L. J. H. Hoffmann, S. Marquardt, C. G. Eisenhardt, H. Baumgartel, R. Chelli, G. Cardini and S. Califano, *Z. Phys. Chem.*, 2004, **218**, 123-153.
52. B. M. Giuliano, A. Maris, S. Melandri and W. Caminati, *J. Phys. Chem. A*, 2009, **113**, 14277-14280.
53. D. J. Hadden, C. A. Williams, G. M. Roberts and V. G. Stavros, *Phys. Chem. Chem. Phys.*, 2011, **13**, 4494-4499.
54. L. J. H. Hoffmann, S. Marquardt, A. S. Gemechu and H. Baumgartel, *Phys. Chem. Chem. Phys.*, 2006, **8**, 2360-2377.

55. R. Matsumoto, K. Sakeda, Y. Matsushita, T. Suzuki and T. Ichimura, *J. Mol. Struct.*, 2005, **735**, 153-167.
56. M. Pasquini, N. Schiccheri, M. Becucci and G. Pietraperzia, *J. Mol. Struct.*, 2009, **924–926**, 457-460.
57. G. Piani, M. Pasquini, G. Pietraperzia, M. Becucci, A. Armentano and E. Castellucci, *Chem. Phys. Lett.*, 2007, **434**, 25-30.
58. G. Pietraperzia, M. Pasquini, N. Schiccheri, G. Piani, M. Becucci, E. Castellucci, M. Biczysko, J. Bloino and V. Barone, *J. Phys. Chem. A*, 2009, **113**, 14343-14351.
59. J. W. Ribblett, W. E. Sinclair, D. R. Borst, J. T. Yi and D. W. Pratt, *J. Phys. Chem. A*, 2006, **110**, 1478-1483.
60. H. Xu and S. T. Pratt, *J. Phys. Chem. A*, 2013, **117**, 12075-12081.
61. V. M. Bhezovskii and E. G. Kapustin, *Russ. J. Gen. Chem.*, 2003, **73**, 401-407.
62. M. Bossa, S. Morpurgo and S. Stranges, *J. Mol. Struct.*, 2002, **618**, 155-164.
63. S. Tsuzuki, H. Houjou, Y. Nagawa and K. Hiratani, *J. Phys. Chem. A*, 2000, **104**, 1332-1336.
64. F. Lahmani, C. Lardeux-Dedonder, D. Solgadi and A. Zehnacker, *J. Phys. Chem.*, 1989, **93**, 3984-3989.
65. D. Xiao, D. Yu, X. Xu, Z. Yu, Y. Du, Z. Gao, Q. Zhu and C. Zhang, *J. Mol. Struct.*, 2008, **882**, 56-62.
66. M. Schreiber, M. R. Silva-Junior, S. P. Sauer and W. Thiel, *J. Chem. Phys.*, 2008, **128**, 134110.
67. G. Grégoire, C. Jovet, C. Dedonder and A. L. Sobolewski, *J. Am. Chem. Soc.*, 2007, **129**, 6223-6231.
68. I. Georgieva, N. Trendafilova, A. J. Aquino and H. Lischka, *J. Phys. Chem. A* 2007, **111**, 127-135.
69. B. Chmura, M. F. Rode, A. L. Sobolewski, L. Lapinski and M. J. Nowak, *J. Phys. Chem. A*, 2008, **112**, 13655-13661.
70. TURBOMOLE, V6.3 2011, a development of University of Karlsruhe and Forschungszentrum Karlsruhe GmbH, 1989-2007, TURBOMOLE GmbH, since 2007; available from <http://www.turbomole.com>.
71. R. Ahlrichs, M. Bär, M. Häser, H. Horn and C. Kölmel, *Chem. Phys. Lett.*, 1989, **162**, 165-169.
72. R. Ahlrichs, *Phys. Chem. Chem. Phys.*, 2004, **6**, 5119-5121.
73. F. Haase and R. Ahlrichs, *J. Comput. Chem.*, 1993, **14**, 907-912.
74. K. Eichkorn, F. Weigend, O. Treutler and R. Ahlrichs, *Theor. Chem. Acc.*, 1997, **97**, 119-124.
75. C. Hättig, *J. Chem. Phys.*, 2003, **118**, 7751-7761.
76. C. Hättig and K. Hald, *Phys. Chem. Chem. Phys.*, 2002, **4**, 2111-2118.

77. C. Hättig and A. Köhn, *J. Chem. Phys.*, 2002, **117**, 6939-6951.
78. C. Hättig and F. Weigend, *J. Chem. Phys.*, 2000, **113**, 5154-5161.
79. A. Köhn and C. Hättig, *J. Chem. Phys.*, 2003, **119**, 5021-5036.
80. T. H. Dunning, *J. Chem. Phys.*, 1989, **90**, 1007-1023.
81. A. Hellweg, C. Hättig, S. Höfener and W. Klopper, *Theor. Chem. Acc.*, 2007, **117**, 587-597.
82. R. A. Kendall, T. H. Dunning and R. J. Harrison, *J. Chem. Phys.*, 1992, **96**, 6796-6806.
83. B. Bogdanov, D. van Duijn, S. Ingemann and S. Hammerum, *Phys. Chem. Chem. Phys.*, 2002, **4**, 2904-2910.
84. S. Azizkarimi, R. Omidyan and G. Azimi, *Chem. Phys. Lett.*, 2013, **555**, 19-25.
85. N. Solcà and O. Dopfer, *J. Chem. Phys.*, 2004, **120**, 10470-10482.
86. E. P. L. Hunter and S. G. Lias, *J. Phys. Chem. Ref. Data*, 1998, **27**, 413-656.
87. G. Parthipan, G. Arivazhagan, M. Subramanian and T. Thenappan, *Phys. Chem. Liq.*, 2011, **49**, 1-8.
88. C.-M. Tseng, Y. T. Lee and C.-K. Ni, *J. Phys. Chem. A*, 2009, **113**, 3881-3885.
89. A. L. Sobolewski and W. Domcke, *Phys. Chem. Chem. Phys.*, 2006, **8**, 3410-3417.
90. A. L. Sobolewski and W. Domcke, *ChemPhysChem*, 2007, **8**, 756-762.

Graphical Abstract:



The CC2 PE profiles of neutral and protonated anisole in the electronic ground and S_1 ($^1\pi\pi^*$) excited state. Excitation of anisole and protonated anisole to the S_1 ($^1\pi\pi^*$) with sufficient excess energy (≈ 5.0 eV), leads the excited systems respectively to the bond cleavage of O-CH₃ and C-OCH₃.